Live births from artificial insemination of microfluidic-sorted bovine spermatozoa characterized by trajectories correlated with fertility

Maria Portia B. Nagata[a], Kenji Endo[b], Kazuko Ogata[c], Kenichi Yamanaka[d], Junki Egashira[e], Naoto Katafuchi[e], Tadayuki Yamanouchi[c], Hideo Matsuda[c], Yuki Goto[c], Miki Sakatani[f], Takuo Hojo[f], Hirofumi Nishizono[g], Kenji Yotsushima[h], Naoki Takenouchi[f], Yutaka Hashiyada[c], and Kenichi Yamashita[a,1]

[a]Advanced Manufacturing Research Institute, National Institute of Advanced Industrial Science and Technology (AIST), Tosu, Saga 841-0052, Japan; [b]Morinaga Dairy Service Co. Ltd., Nasu, Tochigi 329-3224, Japan; [c]National Livestock Breeding Center (NLBC), Nishigo, Fukushima 961-8511, Japan; [d]Faculty of Agriculture, Saga University, Saga 840-8502, Japan; [e]Saga Prefectural Livestock Experiment Station, Takeo, Saga 849-2305, Japan; [f]Kyushu-Okinawa Agricultural Research Center, National Agriculture and Food Research Organization (NARO), Koshi, Kumamoto 861-1192, Japan; [g]Life Science Research Center, University of Toyama, Toyama 930-0194, Japan; and [h]Livestock Research Institute, Toyama Prefectural Agricultural, Forestry & Fisheries Research Center, Toyama 939-2622, Japan

Edited by George E. Seidel, Colorado State University, Fort Collins, CO, and approved February 27, 2018 (received for review October 13, 2017)

Selection of functional spermatozoa plays a crucial role in assisted reproduction. Passage of spermatozoa through the female reproductive tract requires progressive motility to locate the oocyte. This preferential ability to reach the fertilization site confers fertility advantage to spermatozoa. Current routine sperm selection techniques are inadequate and fail to provide conclusive evidence on the sperm characteristics that may affect fertilization. We therefore developed a selection strategy for functional and progressively motile bovine spermatozoa with high DNA integrity based on the ability to cross laminar flow streamlines in a diffuser-type microfluidic sperm sorter (DMSS). The fluid dynamics, with respect to microchannel geometry and design, are relevant in the propulsion of spermatozoa and, consequently, ultrahigh-throughput sorting. Sorted spermatozoa were assessed for kinematic parameters, acrosome reaction, mitochondrial membrane potential, and DNA integrity. Kinematic and trajectory patterns were used to identify fertility-related subpopulations: the rapid, straighter, progressive, nonsinuous pattern (PN) and the transitional, sinuous pattern (TS). In contrast to the conventional notion that the fertilizing spermatozoon is always vigorously motile and more linear, our results demonstrate that sinuous patterns are associated with fertility and correspond to truly functional spermatozoa as supported by more live births produced from predominant TS than PN subpopulation in the inseminate. Our findings ascertain the true practical application significance of microfluidic sorting of functional sperm characterized by sinuous trajectories that can serve as a behavioral sperm phenotype marker for fertility potential. More broadly, we foresee the clinical application of this sorting technology to assisted reproduction in humans.

spermatozoa | rheotaxis | trajectory patterns | fertility | microfluidic sorting

Infertility is a global health issue affecting 48.5–186 million couples worldwide with 20–70% of the cases being attributable to male factors (1). An important approach to counteract male infertility relies on optimum selection of spermatozoa. Spermatozoa need to go through a tenuous journey to reach the fertilization site; thus, motility is seen as one of the most important prerequisites for fertilization. A selection method based on progressive motility that provides a pure population of motile and functionally competent spermatozoa that can achieve beyond fertilization i.e., pregnancy and live birth, is deemed desirable. Clinical evidence supports the concept of paternal contributions to faulty fertilization and aberrant embryo development (2–6), thus highlighting the need for an optimum sperm selection.

Conventional sperm separation techniques involve centrifugation such as the simple wash method, density gradient centrifugation (DGC), the swim-up method, and magnetic activated cell sorting (MACS) used in conjunction with DGC (7–12). However, centrifugation process has potential adverse effects on sperm DNA integrity caused by mechanical damage (13) and excessive levels of oxidative stress by high levels of reactive oxygen species (ROS) that will render the spermatozoa dysfunctional, thereby potentially impairing the fertilization process and embryo development (14). A sperm selection method that separates apoptotic from nonapoptotic spermatozoa based on the externalization of phosphatidylserine residues by magnetic cell sorting (MACS) has been introduced (15). MACS achieved isolation not only of nonapoptotic but spermatozoa with high DNA integrity (16, 17). However, MACS has to be used in conjunction with DGC, and there are contradicting reports on whether to use MACS prior to or after DGC (18, 19) in addition to claim of little benefit in intracytoplasmic sperm injection (ICSI) (20) and lack of significant differences in fertilization, pregnancy, quality of embryos, implantation

Significance

Iatrogenic failures of assisted reproduction technology could be associated with routine sperm preparation techniques. Limitations of conventional sperm selection methods include the inability to efficiently sort functional spermatozoa and assess sperm fertilization potential. We developed a robust microfluidic sperm sorting system by using a diffuser-type microfluidic sperm sorter device capable of ultrahigh-throughput selection and separation of motile, DNA-intact, and functionally competent sperm. The strategy inclusively targeted the intrinsic traits related to fertility and successfully produced livebirths from low-dose insemination of microfluidic sorted spermatozoa. The fertile subpopulation was identified based on the kinetic and trajectory patterns as the sinuous, transitional cohort. The clinical significance of microfluidic sperm sorting is reflected by the established pregnancy and live births of calves.

Author contributions: M.P.B.N. and K. Yamashita designed research; M.P.B.N., K.E., K.O., K. Yamanaka, J.E., N.K., T.Y., H.M., Y.G., M.S., T.H., H.N., K. Yotsushima, N.T., Y.H., and K. Yamashita performed research; M.P.B.N. and K. Yamashita contributed new reagents/analytic tools; K. Yamashita supervised the project; M.P.B.N., K.E., K.O., K. Yamanaka, J.E., N.K., T.Y., H.M., Y.G., M.S., T.H., H.N., K. Yotsushima, N.T., Y.H., and K. Yamashita analyzed data; and M.P.B.N. and K. Yamashita wrote the paper.

The authors declare no conflict of interest.

This article is a PNAS Direct Submission.

[1]To whom correspondence should be addressed. Email: yamashita-kenichi@aist.go.jp.

This article contains supporting information online at www.pnas.org/lookup/suppl/doi:10.1073/pnas.1717974115/-/DCSupplemental.

Published online March 19, 2018.

rates, and live birth rates in samples prepared with or without MACS (21, 22). Another sperm selection method is the nanotechnology-based semen purification which exploits the surface determinants on the dead, defective, and prematurely activated spermatozoa. Separation is achieved by coating magnetic nanoparticles with either antibodies against ubiquitin (23) or lectin that binds glycan exposed at the surface of the sperm with acrosomal damage. Nanopurified bull spermatozoa achieved conception rates equal to those of unpurified semen at half the concentration with no negative effects reported for inseminated cows (24). Increased conception rates occurred in beef cattle inseminated with nanopurified bull semen. However, this technology awaits further investigation, particularly with regard to assurance of complete removal of unbound nanoparticles from purified semen to prevent nanoparticle contamination of the artificial insemination (AI) doses, which then could enter the female reproductive system after insemination.

On the other hand, this paper offers an alternative sperm sorting strategy which is based on microfluidic technology operating on the principles of fluid dynamics in space-constricted environment. This nondamaging approach explored the prospects of sperm rheotaxis: the directed swimming against the direction of flow (25–29). The complete liquid manipulation inside the microchannel system isolated motile and high-quality spermatozoa that are most likely to fertilize the eggs successfully. Sorting relies on the sperm's own ability to swim out of the fluid stream and move through the microchannels, thus reducing the risk of stress-induced damage. In natural conception, biologically, spermatozoa swim through a variable fluidic environment in the female reproductive system that may serve as barrier to the abnormal sperm that cannot swim. Although many of the characteristics of the oviductal environment are impossible to reproduce during sperm sorting, some features such as unidirectional and laminar or gradient flow can be achieved in a microfluidic environment. The idea is to mimic these features and minimize the risk of damage to the spermatozoa, that is, in a sense, a biomimetic sorting mechanism based on sperm motility.

The microfluidic channels permit laminar flow which is characterized by a predictable stream behavior and minimal mixing predominantly by diffusion (30, 31). Engineered microchannels were used to explore the interactions of spermatozoa with structured microenvironments (32), and several studies report on sperm physical interaction with surfaces and walls (27, 33, 34), sperm motion in relation to fluid flows and shear stress (25, 35–37), and dynamics of sperm migration (25, 27, 33–45). Many studies report on microfluidic-based sorting by laminar flow via rheotaxis (25, 35–45). Although almost a quarter-century has passed since the development of the first microfluidic sperm sorter by Kricka et al. (46), and many studies on microfluidic-based sperm sorting technologies followed (25, 35–45), only a few have undergone successful commercialization, and no device has yet been translated to a widely distributed clinical commodity to date. In fact, no microfluidic sperm sorter has been successful in retrieving sufficient number of high-quality spermatozoa that are robust enough to produce pregnancy in AI. To address this problem, we developed a high-throughput microfluidic platform that provides a simple yet efficient tool for the isolation of subpopulations of bull (*Bos taurus*) spermatozoa with desired motility, specific patterns of movement, and functional characteristics. Most sperm sorting technologies simply rely on sperm concentration and motility without much attention on motility pattern recognition. However, our sorting strategy goes beyond mere selection of motile spermatozoa and identifies subpopulations in the sorted population based on trajectory patterns and motility kinematics, which may relate to functional competence and fertility. The pattern of sperm motility with the underlying biological meaning is often overlooked as a potential prognostic fertility factor. We explored the possibility of using visual pattern recognition as a realistic means of predicting the fertilizing ability without subjecting sperm to tedious assays and at the same time making it possible to utilize the sorted sperm for field application.

In humans, only ~10% of the spermatozoa become capacitated (47), and this prompted us to hypothesize that selection of this fertile cohort can achieve successful conception despite low-dose insemination. This concept has been reinforced, ultimately, by our results on comparable pregnancy achieved by insemination of sorted sperm number twenty-fold less than the conventional dose. Although our results demonstrate the tangibility of microfluidic processing in field reproductive programs at the livestock level, it is expected that our sperm sorting strategy may offer great potential in human in vitro fertilization (IVF) or ICSI.

Results

Microfluidic Device Design and Sperm Sorting. The structure and principle of the microfluidic sperm sorting strategy using a diffuser-type microfluidic sperm sorter (DMSS) device is shown in Fig. 1. The biologically inspired microfluidic channel design was created to provide well-defined fluid flow and channel walls that separate each channel. These two features of the microdevice, the fluid flow and channel walls, guide and direct the sperm swimming direction (Fig. 1*D*).

The system is operated by hydrostatic pressure to generate controlled counter-fluid flows through the microchannel system

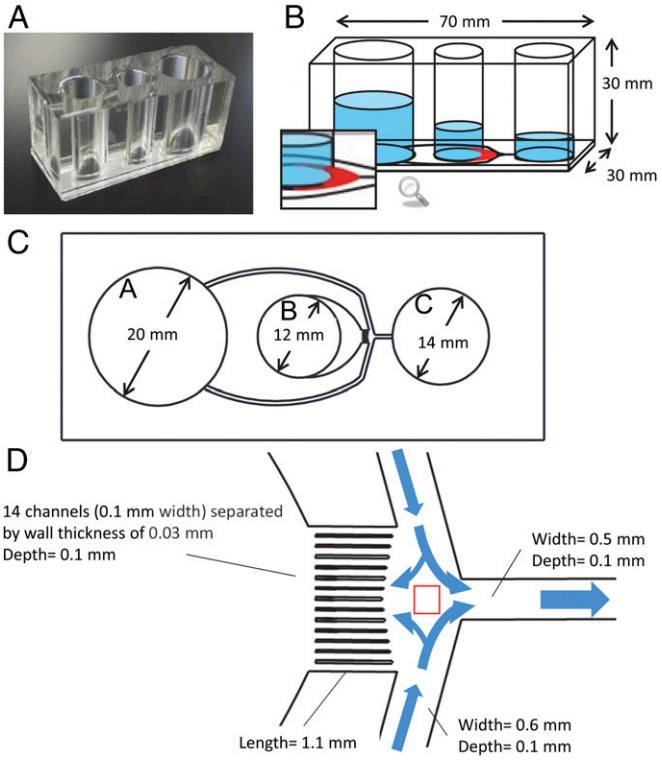

Fig. 1. Photograph and schematic illustration of the DMSS device. (*A*) Photograph of the device composed of PDMS and glass. (*B*) Illustration of microchannels and chambers A, B, and C (sorting medium, semen seeding, and collection, respectively). The crescent shape diffuser is shown in red. (*C*) Microchannel design and geometry from the bottom view of the device. The medium flowing out from chamber A is supplied into chamber B and C. Motile sperm are sorted from frozen–thawed semen in chamber B and accumulated in chamber C; thus, motile sperms are collected from chamber C. (*D*) Magnified illustration of the microchannel network showing the junction area as indicated by the red square. The 14 microchannels separated by walls form laminar flow distribution that flows continuously into crescent-shaped diffuser enabling more motile spermatozoa to swim into this zone, pass through, and travel the distance along the multiple microchannels.

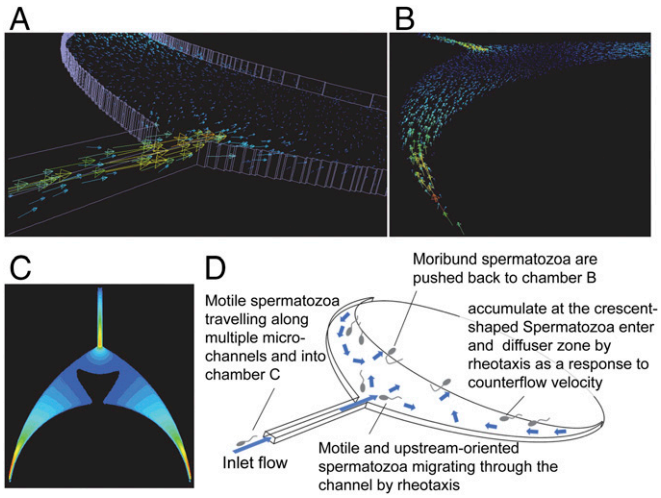

Fig. 2. CFD simulation of the crescent shape diffuser zone and schematic explanation of the motile sperm sorting mechanism. (*A*) Vector image of the countercurrent flow. (*B*) Vector image without the frame line from the different viewpoint from *A*. (*C*) Flow rate magnitude distribution image. Same magnitude color scale is used in *A*–*C*. Higher magnitude is indicated by red, whereas lower magnitude is indicated by dark blue. (*D*) Schematic showing the fluid flow and sperm sorting mechanism. Motile spermatozoa swim upstream at both sides of the diffuser zone and throughout the whole diffuser area and migrate to the center area near the mouth leading to multiple channels. Moribund spermatozoa are pushed back to chamber B, whereas motile spermatozoa are induced by rheotactic property to swim upstream and migrate along the microchannel.

as established from the relative height differences of the liquid column of the three chambers (Fig. 1*B*) and the net capillary force imbalance resulting from the differences in chamber size (Fig. 1*C*). Flow fields with opposite directions are distributed along 14 microchannels and through the crescent shape diffuser, a flow channel with gradually expanding cross-section (Fig. 1*D*), which allows separation of spermatozoa based on their intrinsic ability to cross streamlines in a laminar fluid stream known as rheotaxis. The computational fluid dynamics (CFD) simulation of the crescent shape diffuser (Fig. 2) shows that at relatively faster flow velocities emanating from the connecting multiple channels that create multiple microfluidic flow streams, the speed is gradually decreased by increasing the width of the adjacent crescent shape channel, thus forming a diffuser. When the spermatozoa's moving speed matches the fluid flow speed, the spermatozoa gain the ability to flow against the stream, therefore separating them at different specific positions along the diffuser (Movies S1 and S2). As the diffuser expands approaching the boundary between chamber B (the reservoir of unsorted semen) and the diffuser, the velocity weakens (Fig. 2*C*, black area). The different velocities created in multiple microchannels move into the diffuser while maintaining its energy, hence inducing a large number of spermatozoa to orient themselves against the fluid flow (Movie S1). Such active turning of sperm upstream into the flow allows separation of spermatozoa at different positions along the diffuser zone based on their motility (Movie S2) as mentioned earlier. The countercurrent distributions in the crescent diffuser zone, the first selective filter in the system, allowed migration and separation of spermatozoa from the seminal plasma, immotile and moribund sperm, and debris which remained in the sperm seeding chamber (chamber B). At the narrow-pointed ends of the crescent diffuser, very fast flow velocity is created, which then pulled back the nonmotile and weakly motile sperm cells (Fig. 2 *C* and *D*). A large number of sperm accumulate at the diffuser. The progressively motile spermatozoa after navigating through the diffuser reach the entrance of the multiple channels (all 14 flow channels each separated by a channel wall), which then provide preferential passageways, depending on the swimming velocity of each spermatozoon. Most spermatozoa prefer to align to the wall surface and traverse along the channel wall, whereas a few navigate forward along the channel center surface (Movie S3) as they finally reach the junction (Movie S4) where they are gently swept into the collecting chamber (chamber C) (Fig. 1*D* and Movie S5). Two features that improved the sorting efficiency are the diffuser and multiple channels. The diffuser with its widened area and thus lower flow speed allowed more sperm to be sorted during the first stage of filtering, whereas multiple channels improved the sorting efficiency not only in the quantity but in the quality of sorted sperm.

At the end of the sorting process, a purified high-quality subpopulation of motile spermatozoa (≤1 million) was collected by manually pipetting from chamber C (Movie S5), and AI was performed using the sorted sperm to validate the fertility and predictive utility.

Trajectories and Kinematic Parameters of DMSS-Sorted Sperm. The tracks of DMSS-sorted spermatozoa revealed two distinct subpopulations based on motility pattern trajectories: (*i*) the fast, progressively motile, nonsinuous spermatozoa characterized by symmetrical and moderate-amplitude flagellar beats producing straighter trajectories (PN) (Fig. 3*A* and Table 1) and (*ii*) the transitional type characterized by sinuous trajectory pattern, moderately asymmetrical flagellar beatings, and sinuous trajectories (TS) (Fig. 3*B* and Table 1). Table 1 provides the mean values of kinematic parameters associated with each category recorded for sorted spermatozoa which established successful pregnancy. PN subpopulation with straighter trajectories demonstrates greater mean straight-line velocity (VSL) values than TS subpopulation. Tracks classified as rapid, forward, and progressive are typically very straight with higher linearity (LIN) and higher average path velocity (VAP) as observed in PN compared with TS subpopulation (Table 1).

Results of AI reveal that the population of DMSS-selected spermatozoa with specific motility characteristics and represented by the two identified trajectories at low-dose insemination (≤1 million spermatozoa/insemination) achieved pregnancy rate (13 nonreturn, $n = 35$ inseminated; 37.1%) that is comparable to the conventional unsorted straw (27 nonreturn, $n = 68$, 39.7%) with standard dose (20 million sperm/insemination) in Japanese Black beef cow (data from Morinaga Dairy Service Co.). It is noteworthy to mention that the DMSS-sorted insemination dose was only 5% of the unsorted dose but still achieved positive AI outcome.

Assessment of Field Fertility Relative to AI Timing and Sperm Motility Characteristics Based on Sperm Motion Index of Sorted Sperm. Fig. 4*A* shows sperm motion index (SMI) plots of sorted spermatozoa with respect to pregnancy outcome. This index reflects the intensity of motility of the sorted sperm. Comparison of the mean

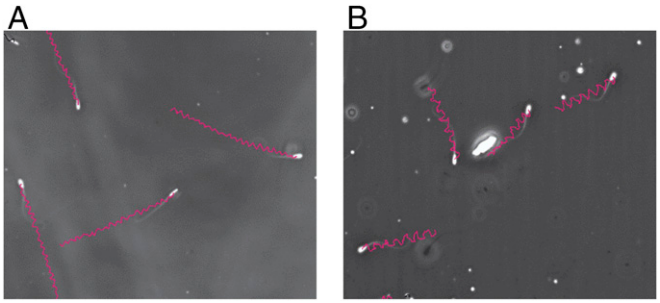

Fig. 3. Typical sperm trajectories of DMSS-sorted bull spermatozoa (*Bos taurus*): (*A*) rapid, linear progressive, nonsinuous (PN) and (*B*) transitional sinuous (TS) with higher SMI and lower SMI used in insemination of heifers, respectively. (Magnification: 150×.)

Table 1. Motion kinematic parameters representing subpopulations of bovine sperm with defined trajectories identified in DMSS-sorted frozen-thawed spermatozoa used in AI which resulted in successful fertilization, pregnancy, and healthy live births

Kinematic parameters	Subpopulations of microfluidic-sorted sperm	
	Rapid linear progressive nonsinuous (PN) (mean ± SD) (range)	Transitional sinuous (TS) (mean ± SD) (range)
VSL, μm/s	89.3 ± 10.7 a (60.1–201.0)	44.5 ± 4.5 b (19.5–98.3)
VCL, μm/s	176.9 ± 25.3 a (55.3–227.2)	120.7 ± 27.3 b (78.8–227.2)
VAP, μm/s	107.8 ± 20.0 a (73.3–205.0)	70.8 ± 25.2 b (21.1–101.3)
STR, %	86.3 ± 4.4 a (44.8–99.8)	68.5 ± 12.7 b (11.7–99)
LIN, %	53.0 ± 2.9 a (42.6–99.9)	40.7 ± 13.2 b (20–60)
ALH, μm	3.5 ± 0.6 a (1.4–12.0)	2.6 ± 0.4 b (1.0–11.8)
BCF, Hz	14.5 ± 1.2 a (9.7–22.0)	9.6 ± 3.4 b (0.8–22.0)
Mean proportion in recovered DMSS-sorted population, %	67.6 ± 2.6	78.6 ± 20.0

Different letters (a and b) indicate significant differences between subpopulations ($P < 0.05$). Two subpopulations (PN and TS) are identified from the whole population of 100% viable and progressively motile DMSS-sorted spermatozoa. Values for each parameter are presented as the mean ± SEM, $n = 5$ for rapid, linear, progressive, and nonsinuous subpopulation, and $n = 5$ for transitional sinuous subpopulation.

SMI values reveals that nonpregnant group has relatively higher values compared with the pregnant group. The ellipse associated to pregnant does not overlap with that of nonpregnant group, thus suggesting that pregnant is relatively different from nonpregnant group with regard to SMI at 95% confidence interval. Our results indicate that sorted sperm that showed low SMI scores have higher tendency to establish pregnancy than those showing a high SMI. This suggests that SMI is associated with the probability of conception and can be used as a reliable predictive index of fertility. Moreover, the prognostic value of SMI reflects its potential use as a new parameter for sperm evaluation.

Pregnancy in relation to SMI and insemination timing is presented in Fig. 4*B*. SMI values were plotted against the timing of insemination from the onset of estrus for pregnant and nonpregnant cows. The graph reveals that successful pregnancies have been achieved by inseminations with DMSS-sorted spermatozoa under two categories based on the interval from onset of estrus: (*i*) 7–8 h period (early AI group, SMI-G1) and (*ii*) 19–27 h period (late AI group, SMI-G2). Approximately 62% of pregnancy belongs to SMI-G2, whereas 32% belongs to SMI-G1. Generally, there seems to be a moderate relationship between SMI and insemination timing. Most pregnancies that were achieved by the late group SMI-G2 involved spermatozoa predominantly exhibiting low SMI (except for the two outliers at 24 and 26 h insemination, which reflected less vigorous motility). However, five remarkable pregnancies occurred when insemination took place early (SMI-G1), wherein there was a wide time span of ovulation, and the sorted spermatozoa exhibited higher SMI reflecting vigorous motility. Although the actual time of ovulation was not determined, timing of insemination was based on window of time relative to observed standing estrus, and ovulation was approximated 30 h after the onset of estrus averaging 27 h.

The slope as shown by the blue line is equivalent to zero reflecting nonpregnancy presumably ascribed to female factors.

This is a report on the application of low-dose insemination of microfluidic-sorted spermatozoa that successfully achieved pregnancy in cattle AI.

Timing of Insemination Relative to Onset of Estrus, Sperm Trajectory Patterns, and Pregnancy. The average diameter of ovulatory follicles was 13.3 mm ± 2.6 mm. The occurrence of ovulation was confirmed on the day after AI. Based on the general scheme of

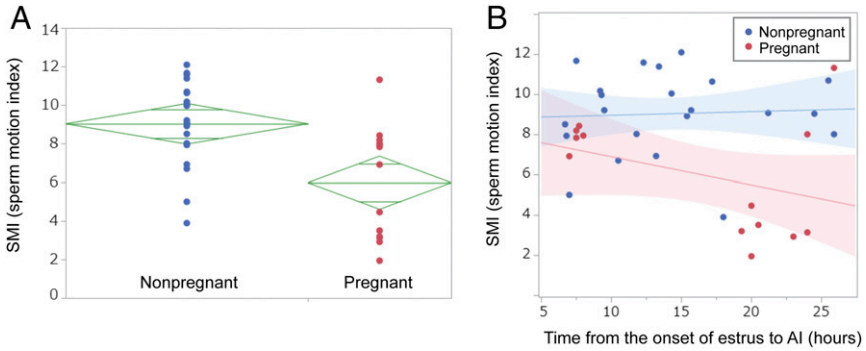

Fig. 4. The SMI distribution of sorted spermatozoa in relation to AI outcome and the effect of SMI and AI timing to pregnancy rate. (*A*) Comparison of SMI distribution of sorted spermatozoa used in AI between pregnant and nonpregnant groups. Diamond mark of each group indicates the following: height, 95% confidence interval; width, sample number of each group; center horizontal line of each diamond mark, average SMI of each group. Two shorter horizontal lines of each diamond mark are overlapped marks. Overlap marks in one diamond that are closer to the mean of another diamond than that diamond's overlap marks indicate that those two groups are not different at 95% confidence interval. Because the overlap marks in one diamond (nonpregnant) are not close to the overlap marks of the diamond of another group (pregnant), they are significantly different at 5% confidence level. (*B*) Correlation between SMI and timing of insemination. Red plots represent sorted spermatozoa resulting in pregnancy after insemination. Red and blue lines are regression lines, and halftone dot meshing indicates 95% confidence interval of each group. Each insemination contains ≤1 million sorted spermatozoa.

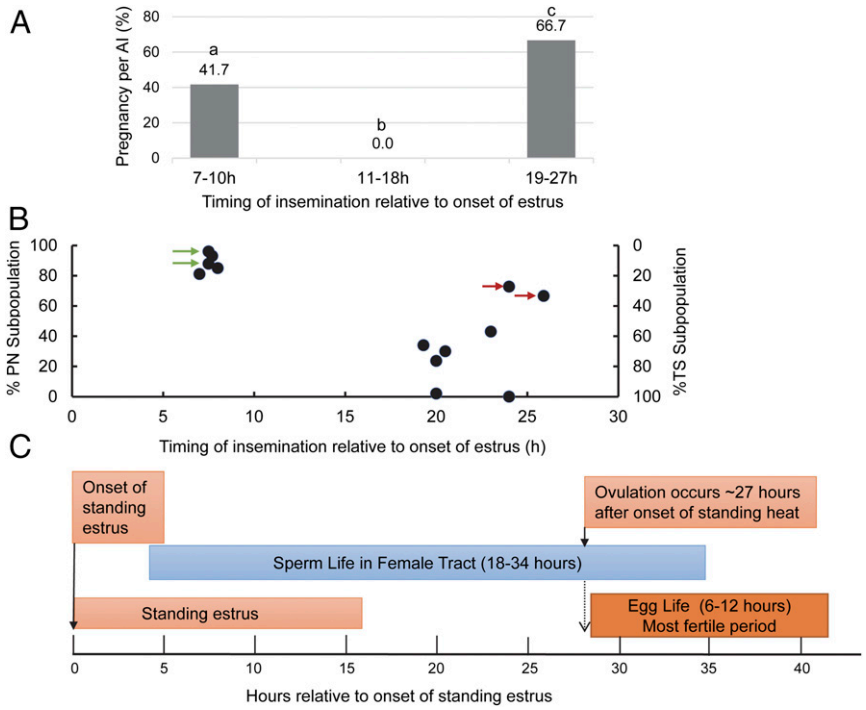

Fig. 5. Biological events associated with AI timing of sorted sperm composed of subpopulations categorized on the basis of kinematic parameters and trajectory patterns. (*A*) Conception rates of cows related to AI timing after estrus onset. The categorical variables were compared using the χ^2 test. $P < 0.05$ were considered statistically significant. Bars without a common superscript differed ($P < 0.05$). (*B*) Correlation between PN and TS subpopulations and pregnancy with respect to AI timing. Nonreturn rates 40 and 60 d after AI were recorded. Red arrows indicate pregnancy with inseminate containing only 30% TS at later AI (24 and 27 h after estrus onset). Green arrows indicate pregnancy of Japanese Black heifers in natural estrus inseminated following the AM–PM rule. (*C*) A guide to time relationships among reproductive events and fertile lifespan of bovine spermatozoa and oocyte.

biological events associated with hours relative to start of standing estrus and ovulation (which generally occurs 24–30 h after onset of estrus, average 27 h) as illustrated in Fig. 5*C*, although the exact time of ovulation is unknown, the insemination schemes were expected to allow sufficient time for sperm transport and capacitation and an overlap of the fertile life of both sperm and egg.

Our results provided insights regarding the importance of time of insemination when using DMSS-sorted sperm in synchronized estrus in cattle. According to the data, the most appropriate time for AI seemed somewhat later (within 19–27 h after estrus onset), as evidenced by the optimal conception rate (~67%), and early insemination produced lower pregnancy conception (~42%) (Fig. 5*A*). No pregnancy at 11–18 h after onset of estrus is intriguing, and thus, insemination at this time is not recommended. These results could be due to the relative proportions of subpopulations types (PN and TS) in the inseminate and their respective capacitation status. Such claim is supported by the analysis of subpopulations of sorted sperm in relation to AI timing. Fig. 5*A* demonstrates the relationship of insemination timing with pregnancy (P/AI) following the use of sorted spermatozoa. Pregnancy rate of ~42% was observed when insemination occurred between 7 and 10 h after onset of estrus, whereas higher pregnancy (~56%) was observed when inseminated between 19 and 27 h after onset of estrus. Surprisingly, cows inseminated 11–18 h after the onset of estrus showed no conception.

Fig. 5*B* presents the percent distribution of PN and TS subpopulations within the sorted sperm population and the respective pregnancies achieved as a function of AI timing. Data show the existence of two groups with respect to pregnancy per AI and timing of insemination: early AI group (7–9 h; $n = 12$) and late AI group (12–27 h; $n = 52$). The plots reveal that when PN predominantly composed the sorted population, pregnancy was achieved when insemination was performed early (7–9 h after onset of estrus). In contrast, sorted sperm with predominant TS subpopulation achieved pregnancy when insemination occurred at a later time (19–27 h after onset of estrus). It is noteworthy to mention that despite the narrow time frame for ovulation (viewed based on the onset of standing heat), insemination that occurred 27 h after onset of estrus, with only 33% TS and predominant PN equivalent to 67%, still produced successful pregnancies (marked by a red arrow in Fig. 5*B*), suggesting that presence of a small fraction of TS subpopulation (33%) is sufficient to establish pregnancy despite insemination occurring late (more likely periovulation). Taken together, these data suggest that TS is more likely the fertilizing cohort that determines fertilization. It should also be noted that even with early insemination producing pregnancy, where PN was predominant, the inseminate contained minimal proportion of TS subpopulation. We are inclined to interpret that PN may likely favor fertilization at early insemination but could not ignore the possibility of TS subpopulation being the fertile fraction because our sorting method could not physically separate these two subpopulations. We therefore deduced that the DMSS-sorted spermatozoa can be specific and, thus, can be applied at early and late insemination.

Assessment of Capacitation Status, Mitochondrial Activity, and DNA Integrity of DMSS-Sorted Spermatozoa. A greater portion of DMSS-sorted sperm exhibited capacitated status (B-patterned) than the unsorted, whereas the number of noncapacitated (F-patterned) was higher in the unsorted than sorted (Fig. 6 *A* and *B*). This difference in the proportion of B-patterned spermatozoa was accounted for by corresponding difference in the proportion of F-patterned spermatozoa, with little difference observed between the treatments upon the proportions of AR-patterned spermatozoa. The enhanced proportion of prematurely capacitated sperm could be attributed to the medium-induced capacitation. The unsorted spermatozoa were

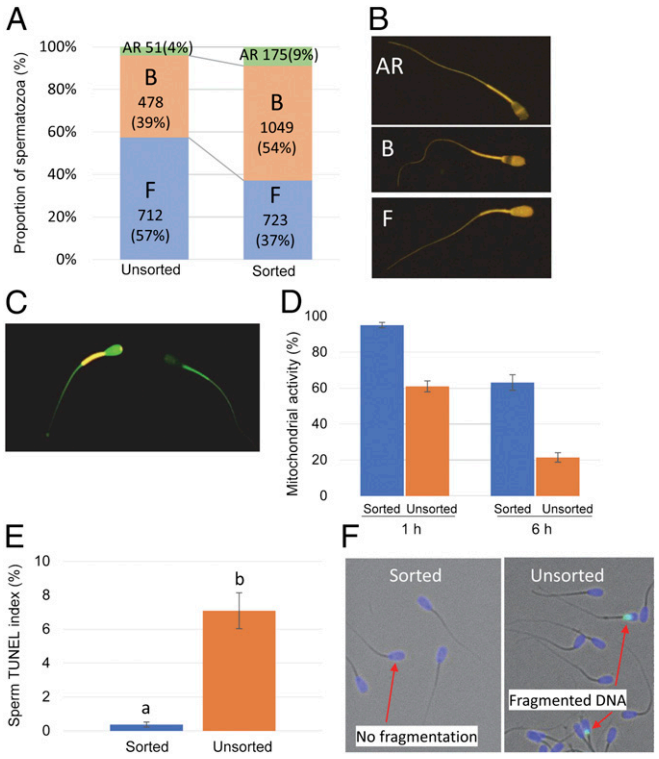

Fig. 6. Assessment of sperm function based on acrosome reactivity, mitochondrial membrane potential, and DNA integrity. (*A*) The proportion of capacitation and acrosome-reacted patterns in sorted bovine sperm assessed by CTC assay. Replicates = 7 (unsorted), 12 (sorted). (*B*) (*Top*) AR pattern corresponds to acrosome-reacted spermatozoa, (*Middle*) B pattern corresponds to capacitated and acrosome-intact spermatozoa, and (*Bottom*) F pattern corresponds to noncapacitated and acrosome-intact spermatozoa. (*C*) Fluorescence photomicrography of sorted spermatozoa stained with JC-1 probe showing orange fluorescence of the sperm midpiece indicating hMMP and green fluorescence indicating low mitochondrial membrane potential. (*D*) Sperm mitochondrial activity expressed as the ratio of sperm with hMMP 1 and 6 h after sorting. Data shown are mean ± SEM (replicates of 7) for 117–136 sperm per replicate of sorted and unsorted sample per replicate. (*E*) DNA fragmentation expressed as the mean sperm TUNEL index (%) of sorted and unsorted sperm. Error bars indicate SD. The results are means ± SD of four sorted and four unsorted samples. The total inspected sperm for sorted samples is 1,925, and for unsorted samples the total is 3,994. Different superscript letters in each bar represent significant differences between samples ($P < 0.01$) detected by a paired t test. (*F*) Sperm nuclei containing DNA fragmentation are detected by TUNEL assay. Each spermatozoon was assigned to contain either normal (blue nuclear fluorescence due to Hoechst 33342) or fragmented DNA (green nuclear fluorescence). (Magnification: *B*, 300×; *C*, 250×; *F*, 200×.)

washed and resuspended in PBS before CTC staining, whereas sorting used a defined capacitating medium: modified Tyrode's medium containing capacitation inducers such as bicarbonate, calcium, and BSA. Moreover, sorting by DMSS could have induced capacitation by excluding seminal plasma which contains decapacitation factors and presumably displaced decapacitation factors from the surface of sperm. These results suggest that sperm microfluidic sperm processing initiated capacitation in half of the sorted population.

Ultimately, however, the best evidence of normal sperm function is successful pregnancy. In terms of pregnancy rate, AI using DMSS-sorted spermatozoa is comparable with the conventional AI using unsorted semen (data from Morinaga Dairy Service Co. Ltd.), with ~40% pregnancy rate (Figs. 4 and 5). It is relevant to note that a low dose of sorted (≤1 million spermatozoa/cow) was utilized in AI, whereas for conventional AI, excessive sperm number (20 million spermatozoa) about 20-fold of the number of sorted spermatozoa was used.

Changes in sperm mitochondrial membrane potential were measured by a sensitive fluorescence probe, 5,5′,6,6′-tetrachloro-1,1′,3,3′-tetraethylbenzimidazolyl carbocyanine iodide (JC-1). The change of color from green to red–orange—that is, JC-1 exists as a monomer at low membrane potential and due to J aggregates turns red–orange at high mitochondrial membrane potential (hMMP)—is shown in Fig. 6*C*. A histogram showing the mean percentages of mitochondrial activity expressed as the ratio of sperm showing hMMP reveals that sorted spermatozoa had higher hMMP than unsorted samples (Fig. 6*D*). The proportions of spermatozoa with high hMMP was 98% for sorted and 60% for unsorted. The mean proportions of hMPP for the sorted and unsorted semen decrease with increasing time as demonstrated by a 30% and 40% decrease in hMMP.

The sperm DNA fragmentation (%) was evaluated as one of the parameters of spermatozoa quality by using the terminal deoxynucleotide transferase-mediated dUTP nick end labeling (TUNEL) (48). The mean total frequency of DMSS-sorted spermatozoa with DNA fragmentation was 0.37% (SD ± 0.15%), a percentage that is significantly lower than the unsorted semen with 7.08% (SD ± 1.06%) DNA fragmentation (Fig. 6*E*). Such remarkable reduction in DNA fragmentation suggests that sperm selection by DMSS allows for effective recovery of not only viable and motile but functional sperm cells with very high DNA integrity.

Discussion

The guiding mechanisms that allow spermatozoa to reach the fertilization site are fundamentally coupled to fluid mechanics (49). We therefore envisaged microfluidic sperm selection: an engineered manipulation of fluid flow in microchannels to isolate undamaged, motile, mature, and physiologically functional sperm with high DNA integrity. Motility sorting was used considering that the self-propelled spermatozoa facilitate upstream navigation by rheotaxis. Studies on upstream swimming of spermatozoa via hydrodynamic transition and microfluidic-based sperm sorting strategies have been reported (25, 35–45). However, these techniques were limited to IVF and ICSI applications due to low number of recovered spermatozoa, and none of these microfluidic methods has been validated in AI setting. Our work, on the other hand, presents an account of high retrieval efficiency of functionally competent sperm cells by microfluidic sorting and its successful application in AI.

The geometry of the microchannels consisting of three filtering zones; the crescent-shaped diffuser, the multichannels, and the junction channel, in synergy with precisely controlled laminar fluid flow velocities, are relevant to prediction of sperm motion, accounting for the variety of sperm displacements and its orientation. The crescent shape diffuser provides the first screening structure. It was observed that spermatozoa are distributed along the diffuser, and their orientations are influenced by the counter-fluid flow velocities (Movie S1). Spermatozoa were seen to reorient and swim against the flow as the flow rate exceeded a critical value, with the sperm swimming trajectories at various flow rates throughout the diffuser zone (Movie S2). This is clearly demonstrated by the sperm head orientations (Movies S1 and S2). Entry of the spermatozoa into the multiple microchannels is a selective process based on their swimming velocity (Movie S3). As spermatozoa travel along the microchannel (Fig. 1*C*, enclosed in red square, and Movie S3), they tend to swim against the sidewalls until they reach the junction where they overcome the final barrier (Fig. 1*D*, enclosed in red square) (Movie S4) and, finally, are gently flushed into the collection reservoir (Movie S5). The filtering process of the DMSS has several features that contribute to AI success. First, DMSS favors progressive motility of cells and effective separation from dead and immotile spermatozoa, debris, seminal proteins, other cells, cryoprotectants, and components of extender present in

the frozen–thawed semen. Selected sperm are 100% viable and motile. Second, DMSS was able to elicit 95% improvement in DNA. Moreover, a striking feature of this sorting method is the ability of low sperm dose (1 million), actually 20-fold less than the conventional unsorted semen to achieve comparable fertility. Pregnancy despite the low dose suggests that the number of inseminated sperm is not a limiting factor provided that high-quality sperm with intact DNA constitutes the inseminate. These results suggest its possible application for the enhancement of semen quality for maximum utilization of subfertile but genetically superior bulls, which are predominantly common in crossbred bulls. This platform can also offer an excellent alternative for the current human sperm sorting methods and is expected to have an effect in IVF and ICSI particularly in terms of excluding the negative effects of dead sperm (ROS generation) and nuclear DNA fragmentation of compromised sperm that may cause fertility impairment. Moreover, semen with low sperm number can benefit from the high-throughput sorting capability of this sperm sorting method using DMSS device.

Another feature of DMSS is the selection of functional subpopulations with specific motility patterns that can serve as a behavioral sperm phenotype marker for fertility. The progressive, space-gaining form of movement of viable spermatozoa is ideally suited to achieving navigation along the diffuser zone and into the microchannels. DMSS not only isolated progressively motile subpopulations but also selected subfractions characterized by two patterns of motility: the linear, progressive trajectory characterized by symmetrical flagellar waves (PN) and the transitional sinuous (TS) type characterized by reduced VSL, decreased linearity, and retained sufficient beat symmetry to maintain progressiveness (TS) (Fig. 3 and Table 1). We examined the relationship between the distribution of PN and TS subpopulations for each successful pregnancy with respect to AI timing and distinguished two groups: the first group (TAI-G1), classified as early AI (7–9 h after onset of estrus) and with predominant PN subpopulation, and the second group (TAI-G2), which was late AI (19–27 h after onset of estrus) and characterized with predominant TS subpopulation (Fig. 5*A*). We found a positive association between predominant PN and pregnancy with respect to early AI in TAI-GI; insemination well ahead of ovulation (ovulation occurs in cows ∼30 h after the onset of estrus) was observed (Fig. 5*B*). A 100% pregnancy rate (two pregnant out of two inseminated) following the AM–PM rule in natural estrus (Fig. 5*B*) was achieved with sorted population composed of predominant PN subpopulation. Considering that spermatozoa have finite lifespans that limit the amount of time before or after ovulation that consequently results in conception and that the sperm responsible for fertilization belongs to the predominant PN subpopulation, the results may imply that longevity of PN is long enough to allow sperm transport, capacitation, and fertilization to occur. On the other hand, the TAI-G2 group demonstrates that TS is significantly correlated with pregnancy when inseminated later, 19–27 h after standing heat, which is more likely near ovulation. In vivo, there are dynamic interactions of spermatozoa with the oviduct that regulate the rate at which they achieve capacitation. Considering that not all spermatozoa are capacitated simultaneously and that there is a need for a continuous replacement of capacitated spermatozoa within a sperm population, these identifications of PN and TS subpopulations may be valuable in predicting fertility of semen, and sorting of these subpopulations at designed proportions may someday prove useful in AI timing using sorted spermatozoa particularly in human intrauterine insemination (IUI). However, at this point, we can only show the trend based on the proportion of each subpopulation in the inseminate and pregnancy data according to insemination groups. We could not, however, isolate these two subpopulations separately for further analysis. An elucidation of the important role of each subpopulation exclusively in the context of capacitation and sperm longevity would provide strong proofs of determinants of fertility but for which no strong data were currently available. The encouraging results of pregnancy by predominant PN at early insemination and predominant TS in late insemination, on the other hand, suggest that the in vivo condition allows in a certain time range these subpopulations that are capable of fertilizing the oocyte once the responsive spermatozoa are in proximity to the cumulus–oocyte complex.

In our attempt to determine the attributes of sperm movement in vitro that correlate with fertility in vivo, we evaluated SMI in relation to pregnancy outcome and found that in general, the mean SMI values for nonpregnant are higher than the pregnant group, whereas those with lower SMI produced successful pregnancies (Fig. 4). Specifically, the pregnant group is divided into two types with respect to AI timing: the first group (SMI-G1), 7–9 h AI with moderate SMI (range: 6.5–8.8), and the second group (SMI-G2), 19–27 h AI with low SMI (SMI range: 2–5) (Fig. 4*B*). However, there are two outliers in the second group depicting moderate and high SMI at 24 and 27 h inseminations, respectively (Fig. 4*B*). This is corroborated with further analysis of the proportion of TS and PN subpopulations as shown in Fig. 5*A* marked with a red arrow indicating that the existence of only about 30% TS (70% PN) is sufficient to achieve pregnancy despite later insemination at 24 or 27 h after onset of estrus. Whether this proportion of TS subpopulation represents an optimal compromise or is crucial for fertility of low-sperm AI needs further study. Nonetheless, our current data provide insights into the possible use of these identified sperm phenotypes in achieving pregnancy in low-dose AI and the possible use of SMI index as a fertility marker. Moreover, there is no ideal method to assess human sperm capacitation and at the same time use the selected sperm in clinical fertilization application such as IUI or IVF. Mere visual observation of these trajectory patterns can allow fertility prediction and, consequently, optimal insemination strategy. We presume that TS subpopulation represents the intermediate category capable of shifting from progressive to capacitated and hyperactivated motility and could be a good predictor of fertilizing ability. These observations on subpopulations with distinctive trajectory patterns representing the fertile group and the SMI index–fertility relations have uncovered a new avenue for researchers to explore. It should be noted, however, that a few cases showing lower SMI failed to establish pregnancy (Fig. 4), which could be attributed to the female factor contributing to nonpregnancy.

Capacitation and acrosome reaction are important prerequisites of fertilization. Spermatozoa acquire the ability to fertilize the oocyte through the process of capacitation during navigation through the female reproductive tract. Moreover, spermatozoa that are naturally in a noncapacitated state should possess the inherent potential to eventually proceed to capacitation upon stimulation. A considerable proportion (54%) of sorted spermatozoa was capacitated. This could be attributed to the sorting medium containing capacitation-supporting components such as bicarbonate, calcium, and BSA, which explains the observed initiation of capacitation. Despite the remarkable percentage of capacitated sperm and the low insemination dosage, pregnancy comparable with the conventional unsorted was achieved, contrary to reports of premature capacitation causing subfertility (50). A plausible explanation could be the role of the elite and uncapacitated spermatozoa composing 37% of the sorted population. Uncapacitated spermatozoa form a reservoir upon reaching the isthmus by binding to the epithelium and establish a quiescent reservoir until they receive a signal associated with ovulation and become capacitated and detach to migrate to the ampulla to fertilize the egg (51). Such interactions carefully regulate the rate at which sperm achieve capacitation so that they are delivered to the surface of the oocyte in a fully primed state, ready for fertilization. The uncapacitated sperm have relatively longer longevity and can plausibly extend the fertile lifespan of the insemination dose, continually replenish a pool of capacitated spermatozoa that can acquire the ability to undergo acrosome reaction, synchronize well with ovulation, and render itself capable of binding and fusion with the oocyte. We cannot, however, measure separately the capacitation status of PN or TS. However,

considering the observation that the proportion of each subpopulation was predominant over the other (Table 1) and given that half of the sorted population is composed of capacitated sperm, then each subpopulation exceeding half of the whole sorted population more likely contains a combination of capacitated and uncapacitated sperm. Each subpopulation may likely be composed of sperm undergoing asynchronous capacitation in vivo, which depends on the age of the sperm and the ability to respond to physiological cues associated with ovulation. Another possibility is the spermatozoa, having undergone the initial stages of capacitation, may not have yet reached the late capacitation stage, and further aging may be minimized in the isthmus, although this claim warrants additional experiments. Capacitation has been reported as a reversible and repeatable phenomenon (52–54), and this holds true for the first stages of capacitation. Capacitation is associated with biochemical changes that include an efflux of cholesterol from the plasma membrane leading to an increase in membrane fluidity and permeability to bicarbonate and calcium ions and hyperpolarization of the plasma membrane. The first stages of capacitation encompass these membrane destabilizing changes, and such activation can be delayed or even reversed by coincubation with membrane proteins of the tubal lining, isthmic fluid, or specific tubal glycoseaminoglycans, such as hyaluronan (55). The attachment of bull spermatozoa to the oviduct and oviductal proteins allows long-term maintenance of motility, and this ability to switch off can delay the induction of the acrosome reaction until the appropriate time. A bovine sperm study gave evidence that the recovery of sperm adhesion is associated with oxidation of sperm-surface protein SH back to SS and the reversal of capacitation (56). In humans, capacitated spermatozoa were used for intrauterine insemination as an alternative treatment for infertility (57–59). In fact, some clinics conduct IUI with ovulation induction using selected and capacitated spermatozoa to patients with infertility problems. We cannot therefore ignore the possibility of capacitating sperm which have not yet reached the late capacitation stage to be functional when AI is timed near ovulation. On the other hand, the uncapacitated subpopulation may provide a continuous replacement of capacitated sperm in the case of a wide window of ovulation time. The optimal time at which insemination should take place relative to ovulation depends on the lifespan of a sufficient number of fertile spermatozoa, the speed of sperm transport and sperm capacitation, and the lifespan of oocyte. The functional integrity and timely transport of spermatozoa in the female genital tract is crucial for maximizing the chance of fertilization and successful pregnancy. With respect to AI timing, there was a tendency for PN to yield pregnancy at early AI, whereas pregnancies were observed with predominant TS subpopulation when inseminated at a later time, and even at a low percentage (22–33% TS), a TS subpopulation was able to ensure pregnancy at later AI. It could be gleaned from our results that TS subpopulation can somehow reflect and predict the fertility of spermatozoa and that sperm trajectory patterns can be used as a prognostic indicator of fertilization ability. Isolation of these fertile subpopulations may uncover a new avenue for researchers to explore specifically on determinants of fertility in the attempt to improve reproduction. Additionally, considering the proportion of capacitated sorted spermatozoa, we believe that the sorting method in adjunct to IVF and ICSI technologies can contribute to reproduction outcome by isolating spermatozoa at the right state of capacitation.

In relation to the putative roles of sperm mitochondria, we evaluated the mitochondrial membrane potential of sorted male gametes as an indicator of the mitochondrial activity status. Although paternal mitochondria are degraded inside the zygote, sperm mitochondria is deemed crucial for sperm function and fertilization. Any alteration in sperm mitochondria that may compromise sperm mitochondrial functionality may potentially affect sperm function and eventually fertilization (60). Sorting enhanced the mitochondrial activity of recovered spermatozoa, and although mitochondrial activity decreased with time, sorted sperm yielded larger hMMP than the unsorted samples. Mitochondrial functionality may also be required for sperm capacitation, and the high hMMP suggests high quality of sorted spermatozoa.

It has been reported that high percentages of progressive motility and DNA integrity in spermatozoa are good predictors of in vitro fertilization capacity (61, 62). Spermatozoa carrying nicked DNA may more likely have a negative effect on fertility, with DNA fragmentation being an uncompensable trait. DNA-nicked spermatozoa showed adverse effects on early embryonic development (63). Our sorting strategy based on sperm rheotaxis suggests that progressive motility may be a highly relevant physiological marker for DNA-intact sperm. The sorting efficiency of DMSS in terms of improvement of DNA integrity was demonstrated by 95% improvement of DNA integrity. This is a significant advancement that can find application in human IVF and ICSI technologies, which bypass the natural sperm selection process in vivo, particularly in ICSI where embryologists choose motile and morphologically normal spermatozoon with no reference to their DNA integrity. However, our microfluidic sperm sorting, an atraumatic method, isolates subpopulations of progressively motile sperm with enhanced DNA integrity. The fragmented DNA accumulated in the nonviable and damaged spermatozoa were eliminated by the selection process. Moreover, the sorting method facilitates exclusion of these dead and moribund cells that cause generation of radical oxygen species (ROS), which damage DNA. In addition, the method eliminates potentially damaging forces such as centrifugation, too rapid flow velocity, dyes, and lasers that cause injury to sperm; thus, the risk of DNA damage has been diminished. Our data on DNA fragmentation were much lower compared with the DNA fragmentation in sex sorted spermatozoa in literature reported (18.4 ~ 21.9%) (64). A comprehensive study on Norwegian Red bulls suggests a significant relationship between DNA strand breaks and bull fertility after AI (65). Considering that sperm DNA alterations may challenge assisted reproduction, selecting spermatozoa using DMSS that give the least possible level of DNA damage will be advantageous.

Summarizing, sperm sorting by DMSS has allowed precise selection of subpopulations with attributes that are concomitantly important determinants of fertility. We were able to isolate and identify spermatozoa that exhibit the optimal physiological features by visual recognition of sperm trajectories related to fertility at the time of insemination and provided a numerical value SMI as a fertility parameter that can be used to evaluate sperm quality. We were able to establish successful pregnancies despite the low dosage and report live births of microfluidic-sorted sperm. Although our device was used to sort bull sperm for AI, we foresee the technique with its capability to reduce the level of DNA damage to be beneficial in human IVF and ICSI. Sperm sorting by DMSS device, therefore, is expected to help solve the male infertility factor by selecting sperm subpopulations with fertile attributes.

Materials and Methods

Reagents. All chemicals were reagent grade and were purchased from Sigma–Aldrich, except for SP-TL buffer, which was purchased from Caisson Laboratories, Inc.; controlled internal drug release (CIDR) device 1900, which was purchased from Pfizer Animal Health; and Spornen and Dalmazin, which were purchased from Kyoritsu Seiyaku Co.

Microchip Fabrication. The DMSS (Fig. 1) was fabricated by micromachining of the poly(methyl methacrylate) (PMMA) master and replica molding using poly(dimethylsiloxane) PDMS following the method published by Briones et al. (66). The microchannel network is composed of two medium-driving channels emanating from chamber A and connected to the junction channel, a flushing channel leading to the outlet and finally into the harvest or collection chamber C, a microstructure adjacent to chamber B which serves as the first area of filtration (crescent-shaped diffuser), and multiple microchannels (composed of 14 channels separated by walls) for the major sorting step, which are connected to the junction channel (Fig. 1 *C* and *D*). The 3D CFD simulation of the crescent-shaped diffuser zone was performed using ANSYS Fluent (ANSYS Inc.) based on a finite-volume scheme. The Euler

mixing model, suitable for mutually miscible fluids, was adopted. For simplicity, however, no slip conditions were assumed in the present study.

Semen samples. Commercially available 0.5-mL straws of cryopreserved semen from 10 Japanese Black beef bulls and 1 Holstein bull were used in microfluidic sperm sorting and AI experiments. Straws containing 20 million sperm per straw were thawed for 30 s at 37 °C in a water bath and processed by microfluidic sperm sorting using the manufactured DMSS microdevice.

Selective sperm sorting by DMSS. The DMSS chambers were filled with modified Sperm-Tyrode's Albumin Lactate Pyruvate (SP-TALP; SP-TL; Caisson Laboratories, Inc.) medium composed of 2.1 mM $CaCl_20.2H_2O$, 3.1 mM KCl, 0.4 mM $MgCl_20.6H_2O$, 100 mM NaCl, 0.29 mM $NaH_2PO_4.H_2O$, 21.6 mM lactic acid, 10 mM Hepes, and 25 mM $NaHCO_3$, 1.0 mM pyruvate, 6 mg/mL BSA (BSA), and 5 mM ethylene glycol-bis(2-aminoethylether)-N,N,N′,N′-tetraacetic acid (EGTA) was used in sperm sorting. The DMSS microdevice has three sorting regions: (*i*) a crescent-shaped diffuser, (*ii*) 14 microchannels separated by walls, and (*iii*) the junction channel (Fig. 1 *A*–*C*). The flow inside the microchannel network was induced by hydrostatic pressure created by the height difference (Fig. 1*B*). A specified sorting protocol was followed on the loading sequence and the volume of semen and buffer to be added into chambers to control the counter-fluid flow and velocities passing through the microchannel system. Sperm sorting using the DMSS device lasted for 30 min.

Evaluation of in vitro motility characteristics of microfluidic-sorted spermatozoa. Approximately 1 mL of sorted spermatozoa was collected, and 5 μL aliquot was used for motility and image analyses using the computer-assisted sperm analysis (CASA) [Sperm Motility Analysis System (SMAS); Ditect Co.], whereas the remaining volume was used in AI. SMAS consists of a computer with sperm analysis software using a five-megapixel CMOS high-speed camera and progressive algorithms. SMAS yields parameters essentially similar to those of other CASA systems such as total sperm count, sperm concentration, percent motility, sperm concentration, curvilinear velocity (VCL), VSL, amplitude of lateral head displacement (ALH), LIN, and beat-cross frequency (BCF).

The slide with the sorted spermatozoa was examined using a 10× negative phase contrast objective and a video camera on a microscope (Nikon Eclipse Ti) fitted with a 37 °C heated stage (Thermo Plate Tokai Hit). Five fields and a minimum of 200 sperm cells at 60 frames per second (fps) were analyzed per specimen. Dynamic parameters were measured in sorted spermatozoa using videomicroscopy and image analysis software. The SMAS instrument captured multiple images and generated tracks of each sperm by marking the head position in 60 frames. The movement characteristics of sperm tracks were subjected to custom category classification.

The SMI was assessed for two categories based on AI pregnancy results: pregnant and nonpregnant groups. To obtain SMI, the velocity parameters VSL and VCL were multiplied and divided by BCF.

Animal experiments. The use of animals was governed by law and notifications of the Japanese Guidelines for Animal Care and Use, and under the administrative guidance of the Ministry of Education, The Morinaga Dairy Service Co. Ltd., NLBC, and Saga Prefectural Livestock Experiment Station followed the rules of the Ethics Committee for the Care and Use of Experimental Animals when animal experiments were being conducted. Moreover, the animal experiments were governed by Law No. 105 and Notification Nos. 6 and 22 of the Japanese Guidelines for Animal Care and Use.

Nulliparous Japanese Black and Holstein heifers were synchronized for estrus by vaginal insertion of a CIDR device (CIDR 1900; Pfizer Animal Health) at arbitrary days of the estrous cycle (day of CIDR insertion = day 0) and 2 mL gonadotrophin releasing hormone (GnRH) (fertirelin acetate; Spornen; Kyoritsu Seiyaku Co.) intramuscularly. Two mL of prostaglandin F2α (PGF 2α) analog (d-Cloprostenol, Dalmazin; Kyoritsu Seiyaku) was administered on day 7, and CIDR device was removed on the morning of day 7. On the ninth day, 2 mL of GnRH was intramuscularly administered, and the animals were observed for the onset of estrus. Sperm sorting was carried out for 30 min, and the sorted spermatozoa were used in AI of cow showing estrus.

Before insemination, the ovaries were examined, and the size of the ovarian follicle was measured by transrectal ultrasonography using an arm-held ultrasound scanner MyLabOne VET (E-SAOTE Veterinary). AI was performed from 7 to 27 h after the onset of estrus judged by standing heat. The occurrence of ovulation was confirmed by rectal palpation on the day after AI.

Pregnancy of two Japanese Black heifers with natural estrus which were inseminated following the AM–PM rule (~7 h after the onset of estrus) is indicated by plots marked with a green arrow, whereas the rest of the plots represent synchronized estrus at Fig. 5*A*.

Pregnancy verification was performed by transrectal ultrasonography after 30 and 50 d of insemination.

Assessment of viability and capacitation status of bovine spermatozoa by combined Hoechst33258/chlortetracycline fluorescence. The dual staining method was performed based on the procedure described by Fraser et al. (67) with some modifications. The chlortetracycline (CTC) fluorescent technique detects changes in the plasma membrane of the bovine spermatozoon (67). Dual staining of spermatozoa with the supravital fluorescent dye (H33258) allows for assessment of cell viability before CTC analysis, hence avoiding the assessment of dead spermatozoa as acrosome reacted cell (68). The three categories used in the classification were F (uniform fluorescent head, intact uncapacitated), B (fluorescence-free band on the post acrosomal region, intact capacitated), and AR (nonfluorescent head or a thin fluorescent band on the equatorial segment, acrosome reacted).

Assessment of sperm mitochondrial activity. Aliquots of DMSS-selected spermatozoa were evaluated for mitochondria membrane potential by the lipophilic cationic probe 5,5′,6,6′-tetrachloro-1,1′,3,3′-tetrathylbenzimidazolecarbocyanine (JC-1) (MitoProbe JC-1 assay kit; Invitrogen), which differentially labeled mitochondria with high and low membrane potentials. JC-1 is a fluorescent probe that can detect at single-cell level variations in mitochondrial membrane potential, by color code. JC-1 changes reversibly its fluorescence from green (monomeric form) when mitochondrial membrane potential is low to orange (multimeric form known as J aggregates) when mitochondrial membrane potential is high (63, 69, 70).

The mitochondrial activity was evaluated under a coverslip with Olympus BX51 fluorescence microscope.

Evaluation of sperm chromatin by TUNEL assay. The nicked DNA in DMSS-sorted and unsorted frozen–thawed spermatozoa was assessed by the terminal deoxynucleotidyl transferase-mediated deoxyuridine triphosphate-nick-end labeling (TUNEL) assay according to the manufacturer's instruction (In Situ Cell Death Detection Kit, Fluorescein; Roche) and as published (48).

Briefly, the unsorted and DMSS-sorted spermatozoa were fixed with 4% paraformaldehyde in PBS on the slides and were washed three times for 5 min with PBS. After fixation, the spermatozoa were permeabilized with 0.1% (vol/vol) Triton X-100 containing 0.1% (wt/vol) sodium citrate for 2 min on ice and washed three times for 5 min with PBS. This was followed by incubation in the dark at 37 °C of 50 μL of TUNEL reaction mixture containing 0.5 IU/μL of calf thymus terminal deoxynucleotidyl transferase, fluorescein-dUTP, and propidium iodide. Spermatozoa treated with RNase-free DNase 1 (400 U/mL; Qiagen) for 10 min at room temperature before incubation with the TUNEL reagent were used as positive control. Negative staining controls received similar treatments except for the absence of terminal deoxynucleotidyl transferase. After incubation, spermatozoa were washed three times with PBS, and coverslips were mounted using mounting medium (VECTASHELD; Vector Laboratories). The TUNEL-positive or TUNEL-negative spermatozoa were observed under a fluorescence microscope (EVOSFL; Thermo Fisher Scientific).

Each sperm was assigned to contain normal or fragmented DNA as indicated by red nuclear fluorescence or intense green nuclear fluorescence, respectively. The DNA fragmentation index determined by the TUNEL assay termed sperm TUNEL index (48) was expressed as a percentage of the total population.

ACKNOWLEDGMENTS. This research work is supported by the Ministry of Agriculture, Forestry and Fisheries, Japan, under the project name "Development of technology for enhancement of livestock lifetime productivity by improving fertility through assisted reproduction." On its fundamental stage, this research is also supported by Japan Society for the Promotion of Science KAKENHI Grant 15H04585 and Adaptable and Seamless Technology Transfer Program through Target-Driven Research and Development (A-STEP) Grant AS242Z00784N from the Japan Science and Technology Agency.

1. Rutstein SO, Shah IH (2004) *Infecundity, Infertility, and Childlessness in Developing Countries*, DHS Comparative Reports No 9 (WHO, Geneva).
2. Barroso G, et al. (2009) Developmental sperm contributions: fertilization and beyond. *Fertil Steril* 92:835–848.
3. Simon L, et al. (2014) Paternal influence of sperm DNA integrity on early embryonic development. *Hum Reprod* 29:2402–2412.
4. Oehninger S, et al. (1988) Failure of fertilization in in vitro fertilization: the "occult" male factor. *J In Vitro Fert Embryo Transf* 5:181–187.
5. Tesarik J (2005) Paternal effects on cell division in the human preimplantation embryo. *Reprod Biomed Online* 10:370–375.
6. Loutradi KE, et al. (2006) The effects of sperm quality on embryo development after intracytoplasmic sperm injection. *J Assist Reprod Genet* 23:69–74.
7. Simon L, Zini A, Dyachenko A, Ciampi A, Carrell DT (2017) A systematic review and meta-analysis to determine the effect of sperm DNA damage on*in vitro*fertilization and intracytoplasmic sperm injection outcome. *Asian J Androl* 19: 80–90.

8. Mortimer D (1991) Sperm preparation techniques and iatrogenic failures of in-vitro fertilization. *Hum Reprod* 6:173–176.
9. Mortimer D (1994) Sperm recovery techniques to maximize fertilizing capacity. *Reprod Fertil Dev* 6:25–31.
10. Pertoft H (2000) Fractionation of cells and subcellular particles with Percoll. *J Biochem Biophys Methods* 44:1–30.
11. Morrell JM, Dalin A-H, Rodriguez-Martinez H (2008) Prolongation of stallion sperm survival by centrifugation through coated silica colloids: A preliminary study. *Anim Reprod* 5:121–126.
12. Said TM, et al. (2005) Advantage of combining magnetic cell separation with sperm preparation techniques. *Reprod Biomed Online* 10:740–746.
13. Alvarez JG, et al. (1993) Centrifugation of human spermatozoa induces sublethal damage; separation of human spermatozoa from seminal plasma by a dextran swim-up procedure without centrifugation extends their motile lifetime. *Hum Reprod* 8: 1087–1092.
14. Aitken RJ, Clarkson JS (1988) Significance of reactive oxygen species and antioxidants in defining the efficacy of sperm preparation techniques. *J Androl* 9:367–376.
15. Grunewald S, Paasch U, Glander HJ (2001) Enrichment of non-apoptotic human spermatozoa after cryopreservation by immunomagnetic cell sorting. *Cell Tissue Bank* 2:127–133.
16. Lee TH, et al. (2010) Magnetic-activated cell sorting for sperm preparation reduces spermatozoa with apoptotic markers and improves the acrosome reaction in couples with unexplained infertility. *Hum Reprod* 25:839–846.
17. Bucar S, et al. (2015) DNA fragmentation in human sperm after magnetic-activated cell sorting. *J Assist Reprod Genet* 32:147–154.
18. Tavalaee M, Deemeh MR, Arbabian M, Nasr-Esfahani MH (2012) Density gradient centrifugation before or after magnetic-activated cell sorting: which technique is more useful for clinical sperm selection? *J Assist Reprod Genet* 29:31–38.
19. Chi HJ, et al. (2016) Efficient isolation of sperm with high DNA integrity and stable chromatin packaging by a combination of density-gradient centrifugation and magnetic-activated cell sorting. *Clin Exp Reprod Med* 43:199–206.
20. Said TM, et al. (2008) Utility of magnetic cell separation as a molecular sperm preparation technique. *J Androl* 29:134–142.
21. Nadalini M, Tarozzi N, Di Santo M, Borini A (2014) Annexin V magnetic-activated cell sorting versus swim-up for the selection of human sperm in ART: is the new approach better then the traditional one? *J Assist Reprod Genet* 31:1045–1051.
22. Romany L, Meseguer M, Gracia-Herrero S, Pellicer A, Garrido N (2010) Magnetic activated sorting selection (MACS) of non apoptotic sperm (NAS) improves pregnancy rates in homologous intrauterine insemination (IUI). Preliminary data. *Fertil Steril* 94: S14.
23. Sutovsky P, Kennedy CE (2013) Biomarker-based nanotechnology for the improvement of reproductive performance in beef and dairy cattle. *Ind Biotechnol* 9:24–30.
24. Odhiambo JF, et al. (2014) Increased conception rates in beef cattle inseminated with nanopurified bull semen. *Biol Reprod* 91:97.
25. Lopez-Garcia MD, Monson RL, Haubert K, Wheeler MB, Beebe DJ (2008) Sperm motion in a microfluidic fertilization device. *Biomed Microdevices* 10:709–718.
26. Smith D, Gaffney E, Blake J, Kirkman-Brown J (2009) Human sperm accumulation near surfaces: A simulation study. *J Fluid Mech* 621:289–320.
27. Denissenko P, Kantsler V, Smith DJ, Kirkman-Brown J (2012) Human spermatozoa migration in microchannels reveals boundary-following navigation. *Proc Natl Acad Sci USA* 109:8007–8010.
28. Tasoglu S, et al. (2013) Exhaustion of racing sperm in nature-mimicking microfluidic channels during sorting. *Small* 9:3374–3384.
29. Tung CK, Ardon F, Fiore AG, Suarez SS, Wu M (2014) Cooperative roles of biological flow and surface topography in guiding sperm migration revealed by a microfluidic model. *Lab Chip* 14:1348–1356.
30. Suh R, Takayama S, Smith GD (2005) Microfluidic applications for andrology. *J Androl* 26:664–670.
31. Beebe D, Wheeler M, Zeringue H, Walters E, Raty S (2002) Microfluidic technology for assisted reproduction. *Theriogenology* 57:125–135.
32. Montenegro-Johnson TD, Gadêlha H, Smith DJ (2015) Spermatozoa scattering by a microchannel feature: an elastohydrodynamic model. *R Soc Open Sci* 2:140475.
33. Nosrati R, Graham PJ, Liu Q, Sinton D (2016) Predominance of sperm motion in corners. *Sci Rep* 6:26669.
34. Elgeti J, Kaupp UB, Gompper G (2010) Hydrodynamics of sperm cells near surfaces. *Biophys J* 99:1018–1026.
35. Schuster TG, Cho B, Keller LM, Takayama S, Smith GD (2003) Isolation of motile spermatozoa from semen samples using microfluidics. *Reprod Biomed Online* 7: 75–81.
36. Cho BS, et al. (2003) Passively driven integrated microfluidic system for separation of motile sperm. *Anal Chem* 75:1671–1675.
37. Hayamizu Y, et al. (2013) Behavior of motile sperm in Taylor-Couette flow: Effect of shear stress on the behavior of motile sperm. *Open J Fluid Dynam* 3:9–13.
38. Eamer L, et al. (2016) Turning the corner in fertility: high DNA integrity of boundary-following sperm. *Lab Chip* 16:2418–2422.
39. Kantsler V, Dunkel J, Blayney M, Goldstein RE (2014) Rheotaxis facilitates upstream navigation of mammalian sperm cells. *eLife* 3:e02403.
40. El-Sherry TM, Elsayed M, Abdelhafez HK, Abdelgawad M (2014) Characterization of rheotaxis of bull sperm using microfluidics. *Integr Biol* 6:1111–1121.
41. Bukatin A, Kukhtevich I, Stoop N, Dunkel J, Kantsler V (2015) Bimodal rheotactic behavior reflects flagellar beat asymmetry in human sperm cells. *Proc Natl Acad Sci USA* 112:15904–15909.
42. Seo D, Agca Y, Feng ZC, Critser JK (2007) Development of sorting, aligning, and orienting motile sperm using microfluidic device operated by hydrostatic pressure. *Microfluid Nanofluidics* 3:561–570.
43. Schulte RT, Chung YK, Ohl LE, Takayama S, Smith GD (2007) Microfluidic sperm sorting device provides a novel method for selecting motile with higher DNA integrity. *Fertil Steril* 88:S76.
44. Asghar W, et al. (2014) Selection of functional human sperm with higher DNA integrity and fewer reactive oxygen species. *Adv Healthc Mater* 3:1671–1679.
45. Shirota K, et al. (2016) Separation efficiency of a microfluidic sperm sorter to minimize sperm DNA damage. *Fertil Steril* 105:315–21.e1.
46. Kricka LJ, et al. (1997) Micromachined analytical devices: microchips for semen testing. *J Pharm Biomed Anal* 15:1443–1447.
47. Cohen-Dayag A, Tur-Kaspa I, Dor J, Mashiach S, Eisenbach M (1995) Sperm capacitation in humans is transient and correlates with chemotactic responsiveness to follicular factors. *Proc Natl Acad Sci USA* 92:11039–11043.
48. Sutovsky P, Neuber E, Schatten G (2002) Ubiquitin-dependent sperm quality control mechanism recognizes spermatozoa with DNA defects as revealed by dual ubiquitin-TUNEL assay. *Mol Rep Dev* 61:406–413.
49. Fauci LJ, Dillon R (2006) Biofluidmechanics of reproduction. *Annu Rev Fluid Mech* 38: 371–394.
50. Kuroda K, Fukushima M, Harayama H (2007) Premature capacitation of frozen-thawed spermatozoa from subfertile Japanese black cattle. *J Reprod Dev* 53: 1079–1086.
51. Suarez SS, Pacey AA (2006) Sperm transport in the female reproductive tract. *Hum Reprod Update* 12:23–37.
52. de Lamirande E, Leclerc P, Gagnon C (1997) Capacitation as a regulatory event that primes spermatozoa for the acrosome reaction and fertilization. *Mol Hum Reprod* 3: 175–194.
53. Mate KE, Harris MS, Rodger JC (2000) Fertilization in monotreme, marsupial and eutherian mammals. *Fertilization in Protozoa and Metazoan Animals: Cellular and Molecular Aspects*, eds Tarin JJ, Cano A (Springer, Berlin).
54. Bedu-Addo K, Lefièvre L, Moseley FL, Barratt CL, Publicover SJ (2005) Bicarbonate and bovine serum albumin reversibly 'switch' capacitation-induced events in human spermatozoa. *Mol Hum Reprod* 11:683–691.
55. Rodriguez-Martinez H (2007) Role of the oviduct in sperm capacitation. *Theriogenology* 68:S138–S146.
56. Gualtieri R, Mollo V, Duma G, Talevi R (2009) Redox control of surface protein sulphhydryls in bovine spermatozoa reversibly modulates sperm adhesion to the oviductal epithelium and capacitation. *Reproduction* 138:33–43.
57. Perino A, Cimino C, Catinella E, Barba G, Cittadini E (1986) In vitro sperm capacitation and intrauterine insemination (IVC-Insem): a simple technique for the treatment of refractory infertility unrelated to female organic pelvic disease. Clinical results and immunological effects: a preliminary report. *Acta Eur Fertil* 17:325–331.
58. Mansour RT, Serour GI, Aboulghar MA (1989) Intrauterine insemination with washed capacitated sperm cells in the treatment of male factor, cervical factor and unexplained infertility. *Asia Oceania J Obstet Gynaecol* 15:151–154.
59. Belker AM, Cook CL (1987) Sperm processing and intrauterine insemination for oligospermia. *Urol Clin North Am* 14:597–607.
60. Amaral A, Lourenço B, Marques M, Ramalho-Santos J (2013) Mitochondria functionality and sperm quality. *Reproduction* 146:R163–R174.
61. Simon L, Lewis SE (2011) Sperm DNA damage or progressive motility: which one is the better predictor of fertilization in vitro? *Syst Biol Reprod Med* 57:133–138.
62. Erickson L, Kroetsch T, Anzar M (2015) Relationship between sperm apoptosis and bull fertility: in vivo and in vitro studies. *Reprod Fertil Dev* 28:1369–1375.
63. Garner DL, et al. (2001) Seminal plasma addition attenuates the dilution effect in bovine sperm. *Theriogenology* 56:31–40.
64. Hu T, et al. (2016) Sperm pretreatment with glutathione improves IVF embryos development through increasing the viability and antioxidative capacity of sex-sorted and unsorted bull semen. *J Integr Agric* 15:2326–2335.
65. Waterhouse KE, et al. (2006) Sperm DNA damage is related to field fertility of semen from young Norwegian Red bulls. *Reprod Fertil Dev* 18:781–788.
66. Briones MPP, et al. (2006) A practical method for rapid microchannel fabrication in polydimethylsiloxane by replica molding without using silicon photoresist. *J Chem Eng of Jpn* 39:1108–1114.
67. Fraser LR, Abeydeera LR, Niwa K (1995) Ca(2+)-regulating mechanisms that modulate bull sperm capacitation and acrosomal exocytosis as determined by chlortetracycline analysis. *Mol Reprod Dev* 40:233–241.
68. Kay VJ, Coutts JR, Robertson L (1994) Effects of pentoxifylline and progesterone on human sperm capacitation and acrosome reaction. *Hum Reprod* 9:2318–2323.
69. Garner DL, Thomas CA, Joerg HW, DeJarnette JM, Marshall CE (1997) Fluorometric assessments of mitochondrial function and viability in cryopreserved bovine spermatozoa. *Biol Reprod* 57:1401–1406.
70. Minervini F, Guastamacchia R, Pizzi F, Dell'Aquila ME, Barile VL (2013) Assessment of different functional parameters of frozen-thawed buffalo spermatozoa by using cytofluorimetric determinations. *Reprod Domest Anim* 48:317–324.